Sensors and Actuators B 208 (2015) 122–127

Contents lists available at ScienceDirect

Sensors and Actuators B: Chemical

journal homepage: www.elsevier.com/locate/snb

Comparative gas sensor response of SnO_2, SnO and Sn_3O_4 nanobelts to NO_2 and potential interferents

P.H. Suman [a], A.A. Felix [a,b], H.L. Tuller [b], J.A. Varela [a], M.O. Orlandi [a,*]

[a] Department of Physical-Chemistry, São Paulo State University, Araraquara, SP 14800-060, Brazil
[b] Department of Materials Science and Engineering, Massachusetts Institute of Technology, Cambridge, MA 02139, USA

ARTICLE INFO

Article history:
Received 12 May 2014
Received in revised form 8 October 2014
Accepted 28 October 2014
Available online 3 November 2014

Keywords:
Tin oxide
SnO_2
SnO
Sn_3O_4
Nanobelts
Gas sensor

ABSTRACT

The gas sensor performance of single crystalline tin oxide nanobelts in different oxidation states (SnO_2, SnO and Sn_3O_4), synthesized by a carbothermal reduction method, is reported. The synthesized materials were characterized by X-ray diffraction, electron microscopy and nitrogen adsorption/desorption experiments. Gas sensor measurements showed that the sensor based on Sn_3O_4 nanobelts exhibits the highest sensor response to 50 ppm NO_2 at 200 °C with an approximately 155-fold increase in electrical resistance. Moreover, at this operating temperature, Sn_3O_4 nanobelts were found to display the highest selectivity to NO_2 relative to CO while SnO nanobelts exhibited the highest selectivity to NO_2 relative to H_2 and CH_4. These results show that tin oxide semiconducting nanomaterials, with the unusual oxidation states of SnO and Sn_3O_4, show great promise as alternatives to SnO_2 for use in high performance gas sensor devices.

1. Introduction

The development of chemical sensors with improved sensitivity has been greatly accelerated in recent years with the introduction of semiconductor nanostructures with optimized morphologies [1]. Such devices show promise for detecting pollutant gases at ppm, and even ppb levels, with high sensitivity, selectivity and response speed [2], thereby potentially satisfying a wide range of requirements in the safety, health, environment and energy conservation areas [3,4]. SnO_2 is a wide band gap n-type semiconductor [5,6], and among many metal oxides studied for gas sensors applications [7–11], is one of most investigated materials [12]. Due to its excellent thermal and chemical stability at different atmospheres, engineered SnO_2-based gas sensors have been used for the detection of different gases [13–16] taking advantage of chemical and/or morphological modifications and optimization of operating conditions.

While SnO_2 is the most studied and best known gas sensing material, the gas sensor properties of tin oxides with other oxygen stoichiometries (e.g., SnO and Sn_3O_4) have very recently been reported [17–19]. This delay in examination of these other tin oxides is not surprising given the difficulty in synthesizing these phases and their thermal instability at high temperatures (above 400 °C for SnO [20,21] and above 500 °C for Sn_3O_4 [22]). SnO is reported to exhibit p-type conductivity, an indirect band gap of approximately 0.7 eV and a direct band gap of 2.7 eV and is found to crystallize in orthorhombic or tetragonal structures [23,24]. The gas sensor properties of tetragonal single crystalline SnO micro-disks, synthesized by a carbothermal reduction method, were recently reported, for the first time, by the authors [17]. These materials were found to exhibit an approximately 1000-fold response to 100 ppm NO_2. This so-called Giant Chemo-Resistance (GCR) response was attributed to the existence of a high density of active lone pair electrons on the exposed (0 0 1) planes of the SnO structure. Even less examined than SnO, Sn_3O_4 is an intermediate tin-oxide phase lying between SnO and SnO_2 [25]. The authors also reported, for the first time, the gas sensor properties of single crystalline Sn_3O_4 nanobelts, synthesized by a carbothermal reduction method [18]. These nanostructures displayed n-type semiconductor behavior and good sensitivity to O_2. Given the initial attractive sensor response reported for both SnO and Sn_3O_4, the gas sensor performance of these new alternative tin oxide based materials merit closer examination, particularly in comparison to the response of the standard SnO_2 sensor material.

In this work, a comparative study of the gas sensor properties of SnO_2, SnO and Sn_3O_4 nanobelts synthesized by carbothermal reduction is presented. As demonstrated below, both SnO and Sn_3O_4 nanobelts exhibit higher sensitivity and selectivity relative

* Corresponding author at: Department of Physical-Chemistry, São Paulo State University – UNESP, Rua Francisco Degni 55, Quitandinha, P.O. Box 355, Araraquara, SP CEP: 14800-060, Brazil. Tel.: +55 16 3301 9644; fax: +55 16 3322 0015.
E-mail address: orlandi@iq.unesp.br (M.O. Orlandi).

http://dx.doi.org/10.1016/j.snb.2014.10.119
0925-4005/

to potential interferent gases (H_2, CO and CH_4) than SnO_2 nanobelts. These observations suggest that these lower oxidation state tin oxides represent a new class of promising materials with exceptional gas sensor performance.

2. Experimental

Tin oxide nanobelts in different oxidation states were synthesized by a carbothermal reduction method using a mixture of SnO_2 powder (Sigma–Aldrich, 99.9% purity) and carbon black (Union Carbide, >99% purity) in the molar ratio of 1.5:1 (SnO_2:C) as starting material. This mixture was used in two synthesis runs performed at 1135 °C for 75 min, but with different synthesis atmospheres. In one synthesis, a nitrogen gas flow of 80 sccm was used to ensure an inert synthesis atmosphere. In another synthesis, a controlled oxidizing synthesis atmosphere was established by using a nitrogen gas flow of 150 sccm and an oxygen gas flow of 0.5 sccm, which was introduced in the counter-flow of nitrogen gas when the temperature reached 900 °C. Optimized parameters used and experimental details of these syntheses are described in detail in our previous reports [18,26]. Following both syntheses, wool-like materials with different colors (dark gray, white and yellow) were removed from the inner walls of the alumina tube in different regions, i.e., materials grown at different temperatures. In an inert synthesis atmosphere, the dark material was collected in the tube region where the temperature was about 350 °C and both SnO nanobelts and micro-disk structures were obtained. Due to the size difference between these structures, it was possible to separate them by sedimentation in isopropyl alcohol. The SnO nanobelts, the morphology of interest in this study, were dried at 50 °C following separation procedure. Both SnO_2 (white material) and Sn_3O_4 (yellow material) nanobelts were obtained when using an oxidizing synthesis atmosphere in the tube region where the temperature was about 500 °C and 700 °C, respectively.

The morphological characteristics of the nanobelts were examined by field emission scanning electron microscopy (FEG-SEM; JEOL, model JSM-7500F) and the phase and the crystallinity of the nanobelts were studied by X-ray diffraction (XRD; Shimadzu, model XRD 6000) using CuKα radiation. Specific surface area was determined by the Brunauer–Emmett–Teller method (BET) [27] under N_2 adsorption/desorption experiments (Micromeritics instrument, model ASAP 2000). For gas sensing measurements, the collected materials were separately dispersed in isopropyl alcohol with the aid of an ultrasonic cleaner. Several drops of each suspension containing the nanobelts were directly dropped onto alumina substrates coated with interdigitated platinum electrode arrays (100 μm Pt fingers spaced 200 μm apart). The substrates were then heated to 100 °C for 15 min to evaporate the solvent. The substrates were then inserted in a tube furnace capable of measuring the gas sensor response of 8 materials in parallel, thereby enabling a comparison of the sensor response of different materials under near identical conditions. Gas sensing tests were carried out by applying a direct voltage of 0.1 V and monitoring changes in the electrical resistance (using an HP34970A data acquisition multiplexer unit) during cyclic exposure to different concentrations of NO_2 (between 1 and 50 ppm) and H_2, CO and CH_4 (between 10 and 500 ppm) diluted in dry air (baseline gas) with the aid of mass flow controllers (MKS). The total gas flow rate (test plus balance gas) was maintained constant (200 sccm) during all tests. The sensor test devices were equilibrated in dry air for 12 h at each temperature before the beginning of each gas sensor measurement to insure a stable and reproducible baseline resistance. Gas sensor measurements were performed in the range from 150 to 350 °C, with steps of 50 °C, to insure thermal stability of these materials. The sensor signal, which represents the magnitude of the change of the electrical resistance of the nanobelt arrays, was defined as R_{gas}/R_{air} for oxidizing gases where R_{gas} is the electrical resistance measured when the materials were exposed to the analyte gas and R_{air} is the electrical resistance measured in the air reference (baseline gas). The sensor signal for reducing gases is defined instead by R_{air}/R_{gas}. The response (recovery) time was defined as the time needed to reach 90% of the final steady state electrical resistance following exposure (removal) to (of) the analyte gas [28,29].

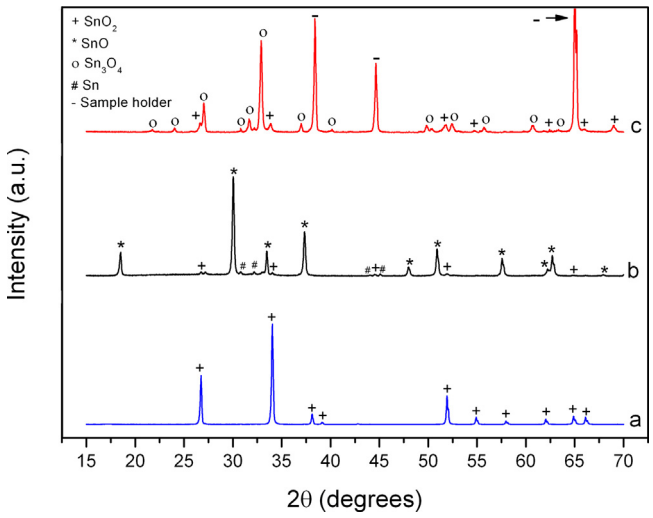

Fig. 1. XRD patterns of as synthesized materials. (a) white, (b) dark and (c) yellow material.

3. Results and discussion

Fig. 1 shows the XRD patterns of as synthesized materials. The white material (Fig. 1a) presents only the cassiterite SnO_2 phase peaks with clear evidence for (101) orientation (peak at 33.9°). For the dark material obtained after the synthesis, Fig. 1b shows contributions largely from the SnO phase with minor contributions from SnO_2 and Sn. For the yellow material, Fig. 1c shows peaks large from the Sn_3O_4 with minor contributions from SnO_2. Sample holder peaks are also observed in Fig. 1c. Based on the above results, it is shown that controlling the synthesis conditions it is possible to obtain structures in different tin oxidation states.

Fig. 2a–c shows FEG-SEM images of the tin oxide nanobelts in the different oxidation states. Nanobelts, grown in all three phases, have relatively uniform widths along their length with the maximum width distribution centered in the range of 20–30, 50–100 and 100–150 nm for SnO, SnO_2 and Sn_3O_4 nanobelts, respectively and lengths of the order of dozens of microns or even millimeters. Furthermore, the surfaces of the nanobelts are flat and smooth [24,26], though the Sn_3O_4 belts present a layered surface [18]. The presence (or not) of metallic spheres at one extremity of the nanobelts is related to their growth mechanisms, which occurs by a self-catalytic vapor–liquid–solid (VLS) process [24,26,30] for SnO nanobelts (the Sn peak at XRD is related to the catalytic metal) and by vapor–solid (VS) process [31,32] for both SnO_2 and Sn_3O_4 nanobelts. Moreover, these belts were also characterized by XRD and TEM [18,24,31] showing that they are single crystalline and SnO_2 nanobelts grow in the (1 0 1) plane of tetragonal structure, SnO nanobelts grow in the [1 1 0] direction of orthorhombic structure, and Sn_3O_4 nanobelts growth is related to the (1 0 1) plane of triclinic structure.

Measurements of the gas sensor response showed the electrical resistance (R_{gas}) of all nanobelts to increase after exposure to different levels of NO_2 and decrease after exposure to all levels of H_2, CO and CH_4 (not shown here). This is a typical behavior of n-type

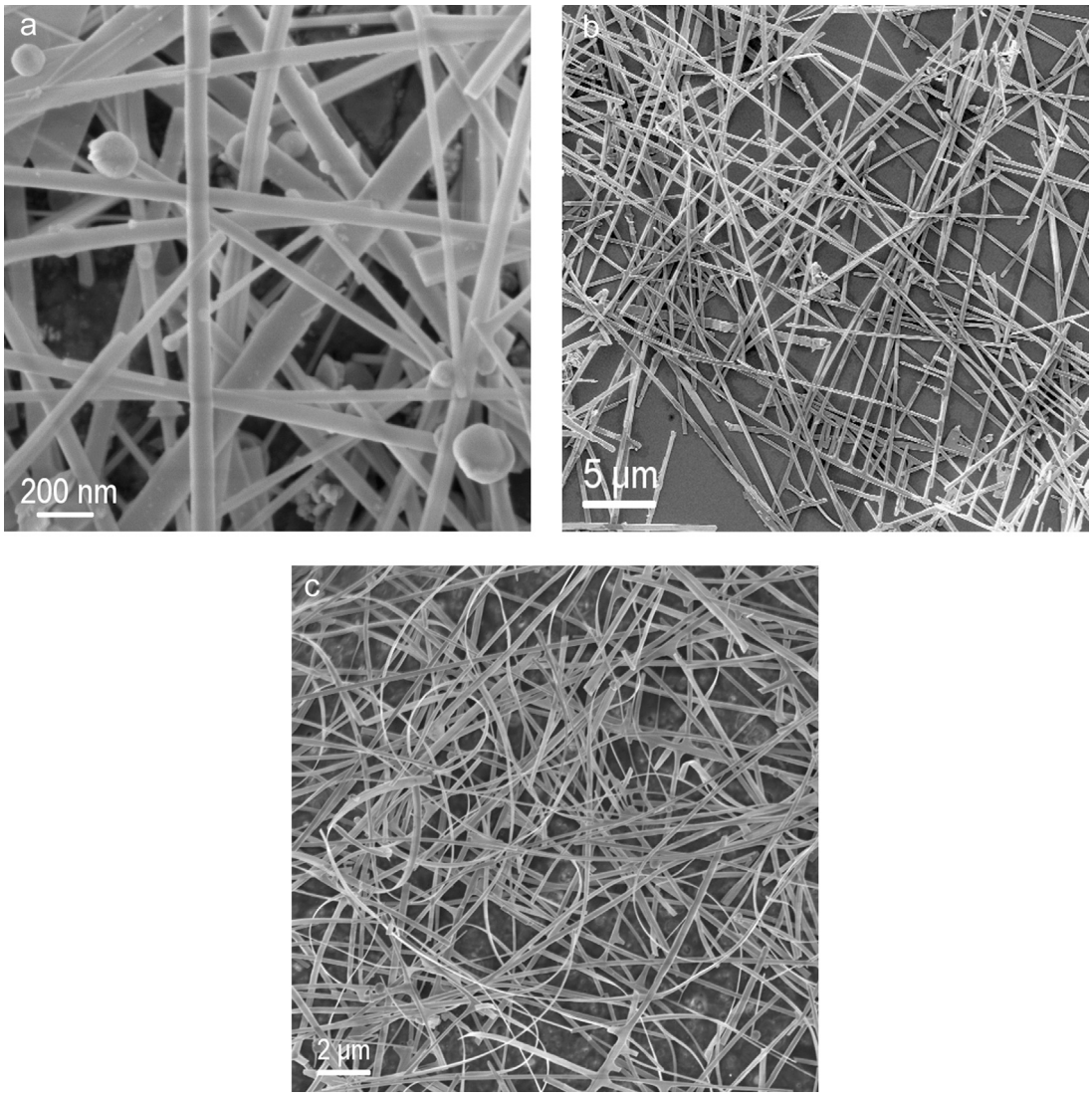

Fig. 2. FEG-SEM images of (a) SnO, (b) SnO_2 and (c) Sn_3O_4 nanobelts synthesized by a carbothermal reduction method under controlled synthesis atmospheres.

semiconductor materials, well known for SnO_2 [5], and consistent with results obtained in previous work for SnO micro-disks [17] and Sn_3O_4 nanobelts [18]. SnO materials are usually reported in the literature to be p-type semiconductor [19,23], possibly due to the presence of tin vacancies [33]. However, as the SnO nanobelts investigated in this study were synthesized by a carbothermal reduction method under a reducing atmosphere, and this material is likely oxygen deficient and therefore exhibits n-type behavior. Similarly, Sn_3O_4 nanobelts were formed in a region with oxygen deficient atmosphere; thus n-type behavior is also expected. Additional experiments are underway to examine this question regarding the relation between carrier type and concentration and the degree of oxygen nonstoichiometry in these compounds.

Fig. 3 shows the sensor signal of the tin oxide nanobelts in the different oxidation states taken at 200 °C, as a function of time, in response to periodic 20 min long NO_2 pulses, with concentrations ranging from 1 to 50 ppm. For all the materials, the sensor signal increased by increasing NO_2 concentration, showing that no saturation was obtained in this range. For 1 and 2 ppm of NO_2 the sensor response of SnO and Sn_3O_4 are similar and much higher than the SnO_2 response. As SnO belts are thinner than Sn_3O_4 they should be more depleted for low gas concentration, having a higher sensor signal. As the NO_2 concentration increases, the influence of analyte

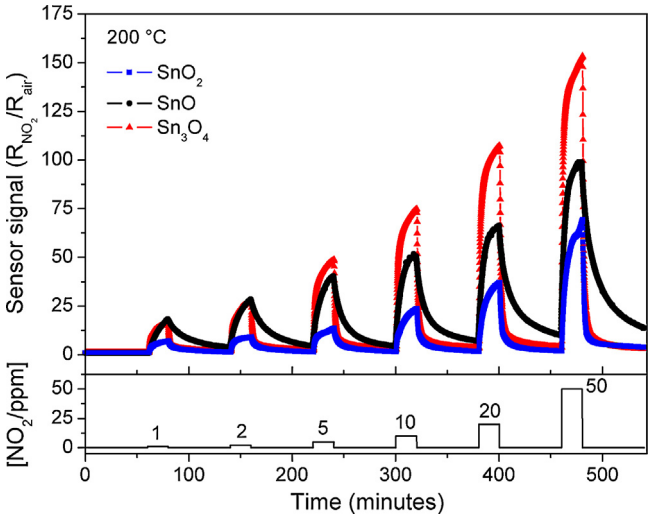

Fig. 3. Sensor signal vs. time of the tin oxide nanobelts in the three different oxidation states, at 200 °C, during cyclic exposure to periodic 20 min long NO_2 pulses, with concentrations ranging from 1 to 50 ppm. The sensor signal is defined as R_{gas}/R_{air} to NO_2 and R_{air}/R_{gas} to reducing gases (H_2, CO and CH_4).

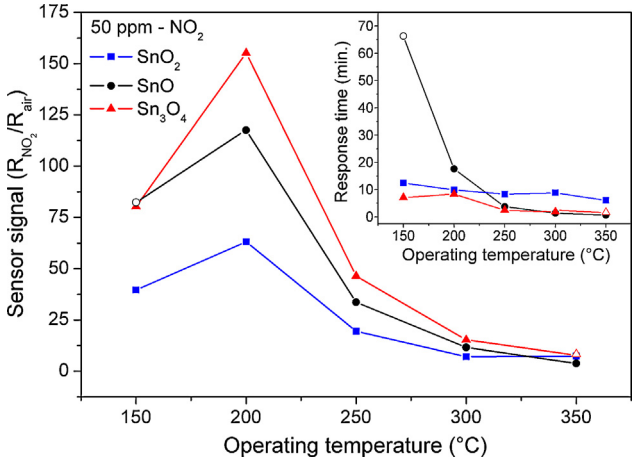

Fig. 4. Sensor signal vs. operating temperature of tin oxide nanobelts at 50 ppm NO_2 in dry air. The inset shows the response time of the tin oxide nanobelts to 50 ppm of NO_2 as function of the operating temperature. The response time is defined as the time needed to reach 90% of the final steady state electrical resistance following exposure to the analyte gas. (The open points for SnO material at 150 °C and for Sn_3O_4 material at 350 °C means that these values were obtained in a different sample than other points.)

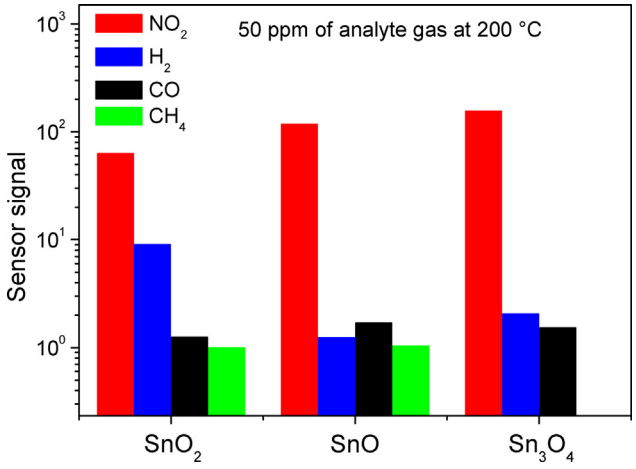

Fig. 5. Sensor signal of the three tin oxide nanobelts compositions for 50 ppm of NO_2, H_2, CO and CH_4 at 200 °C.

gas adsorbed on belts surface becomes more effective on the depletion layer of Sn_3O_4 and its sensor signal overtake the SnO one, being almost 1.5 higher than the SnO sensor signal for 50 ppm of NO_2. In this way, the sensor based on Sn_3O_4 nanobelts clearly exhibited the highest response for NO_2 levels greater than 5 ppm, as compared to the responses of SnO and SnO_2 nanobelts, with an approximately 17-fold increase in resistance when exposed to 1 ppm NO_2 and approximately 155-fold increase in resistance to 50 ppm NO_2. It is important to notice that the sensing response of the SnO_2 nanobelts was lower than both the SnO and Sn_3O_4 responses for all levels of NO_2. Furthermore, as observed in Fig. 3, the kinetics of adsorption of the analyte gas appears to be similar for all three materials, unlike kinetics of desorption (recovery process) which seems to be slower for the SnO than for SnO_2 and Sn_3O_4 nanobelts. A possible explanation for this fact is addressed below.

The sensor signal was found to follow a power law dependence on gas concentration as $R \propto p_{NO_2}^{\beta}$, with β taking on the values of 0.44, 0.56 and 0.50 for SnO, SnO_2 and Sn_3O_4 nanobelts, respectively. Assuming that this dependence continues to hold to lower NO_2 concentrations, a sensor response of ~7, ~2 and ~7 to SnO, SnO_2 and Sn_3O_4 nanobelts, respectively is estimated for an exposure to 100 ppb of NO_2 [10,11]. These results easily satisfy the National Ambient Air Quality Standards (NAAQS) requiring detection of 100 ppb per hour, the standard set for public health protection by the U.S. Environmental Protection Agency [34].

Fig. 4 shows the sensor response to 50 ppm NO_2 as a function of operating temperature. The optimum operating temperature with respect to the maximum sensitivity is in the range of 200 °C for all nanobelts. This is well below their decomposition temperatures, pointing to the long term stability of these nanostructures under these operating conditions. This volcano-like response is likely the consequence of the competition between slow gas adsorption kinetics of molecular species at lower temperatures and enhanced desorption of atomic species at higher temperatures [28]. Due to experimental issues, no sensor response was obtained for Sn_3O_4 nanobelts at 350 °C. The inset in Fig. 4 presents the response time of the tin oxide nanobelts to 50 ppm of NO_2 as function of the operating temperature. For all materials, the response time decreases with increasing temperature, which is expected due to faster adsorption/desorption processes at higher temperatures. Means for reducing the response time of approximately 10 min at 200 °C deserves further attention.

The selectivity of the three different tin oxide nanobelt compositions to NO_2 versus other potential interferent gases was also investigated. Fig. 5 shows the sensor response of SnO, SnO_2 and Sn_3O_4 nanobelts to 50 ppm of NO_2, H_2, CO, and CH_4 in air at 200 °C. All of the tin oxide nanobelts are observed to exhibit selectivity to NO_2 relative to the other common interferent gases. The results show that the SnO nanobelts exhibit the highest selectivity to NO_2 relative to H_2 and CH_4, with values of sensor response approximately 95-fold larger for NO_2 than for H_2 and approximately 115-fold larger for NO_2 than for CH_4. Furthermore, Sn_3O_4 nanobelts exhibit the largest selectivity to NO_2 relative to CO with values of sensor response more than 100-fold larger for NO_2 than for CO. On the other hand, SnO_2 nanobelts showed the lowest values of selectivity for NO_2 compared to H_2, CO and CH_4.

It is well known that the gas sensor performance is dependent on the specific surface area of the sensor material [35,36]. Li et al. [37], for example, showed a linear relationship between the surface areas of SnO_2 and their gas sensitivities to H_2 and CO. Accordingly, nitrogen adsorption/desorption experiments were performed and the specific surface areas of the tin oxide nanobelts were determined by the Brunauer–Emmett–Teller (BET) method [27] to test this relationship. Fig. 6 shows the N_2 isotherms of the tin oxide nanobelts, and according to IUPAC classification these isotherms

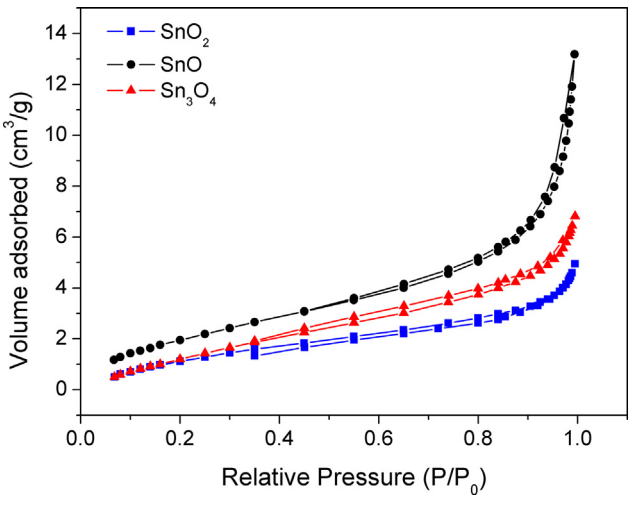

Fig. 6. Nitrogen adsorption/desorption isotherms for tin oxide nanobelts.

are of type II, characteristic of non-porous or macroporous (>50 nm) materials [38]. In fact, as noted in the FEG-SEM images (Fig. 2) the surfaces of the nanobelts are smooth and without any evident defects, i.e., they are non-porous structures. The specific surface areas of the SnO, SnO_2 and Sn_3O_4 nanobelts were determined to be 8 $m^2 g^{-1}$, 6 $m^2 g^{-1}$, 7 $m^2 g^{-1}$, respectively. In addition to the non-porous character of these structures, the relatively low values of specific surface areas can be related to the length of the nanobelts that may be of the order of micrometers or even millimeters. These results indicate that all tin oxide nanobelts have similar surface areas, so it should not be the determining factor in their relative gas sensor response. On the other hand, as pointed out before, the smaller size of SnO belts enables these belts to be more easily depleted presenting a higher sensor signal at low concentrations. Moreover, recent density functional theory (DFT) calculations of SnO and Sn_3O_4 structures indicate the presence of lone pairs on their surfaces [39,40]. These lone pairs are particularly active sites for oxidizing gases, such as NO_2, and so can explain the superior performance of SnO and Sn_3O_4 nanobelts in comparison to the SnO_2 standard material. Thus, the whole sensor response of a material is the synergic effect of exposed surface, material size and the presence of lone pairs, providing to SnO and Sn_3O_4 belts the advantage to have lone pairs on their exposed surface.

The lone pairs can also be important relative to the low recovery time of SnO belts. It is known that SnO has a high density of lone pairs on (0 0 1) surface [39] so it can be less favorable for desorption of gases, increasing the recovery time of this material.

Given their superior performance, more studies addressing these lower oxidation state non-stoichiometric tin oxide structures are merited, with the objective of developing a deeper understanding of the sensor response of these materials.

4. Conclusions

A comparative study of the gas sensor response of SnO_2, SnO and Sn_3O_4 nanobelts, synthesized by a carbothermal reduction method, was presented. The nanobelts of all the tin oxide based materials exhibit a maximum in sensitivity to NO_2 at 200 °C, with the highest sensor signal observed for Sn_3O_4 followed by the SnO and SnO_2 nanobelts, respectively. Furthermore, exceptional selectivity against potential interferent gases such as H_2, CO and CH_4 was also obtained. Our results show that SnO and Sn_3O_4 materials exhibit superior NO_2 detection than the SnO_2 standard for similar morphologies and that these nanostructures show promise for use in high performance gas sensors devices.

Acknowledgements

The authors acknowledge the São Paulo Research Foundation (FAPESP) (Procs. 2009/13491-7 and 2010/51959-8), and The National Council for Scientific and Technological Development (CNPq) (Proc. 200703/2011-3) for financial support of the MISTI MIT-Brazil Seed Fund. TEM and FEG-SEM facilities were provided by the IQ-UNESP. The authors have no competing financial interests related to this work.

References

[1] I.D. Kim, A. Rothschild, H.L. Tuller, Advances and new directions in gas-sensing devices, Acta Mater. 61 (2013) 974–1000.
[2] N. Yamazoe, N. Miura, Environmental gas-sensing, Sens. Actuators: B 20 (1994) 95–102.
[3] N. Yamazoe, Toward innovations of gas sensor technology, Sens. Actuators: B 108 (2005) 2–14.
[4] E. Comini, Metal oxide nano-crystals for gas sensing, Anal. Chim. Acta 568 (2006) 28–40.
[5] Z.M. Jarzebski, J.P. Marton, Physical-properties of SnO_2 materials. 1. Preparation and defect structure, J. Electrochem. Soc. 123 (1976) C199–C205.
[6] S. Munnix, M. Schmeits, Electronic-structure of tin dioxide surfaces, Phys. Rev. B 27 (1983) 7624–7635.
[7] J. Zhang, S.R. Wang, M.J. Xu, Y. Wang, B.L. Zhu, S.M. Zhang, W.P. Huang, S.H. Wu, Hierarchically porous ZnO architectures for gas sensor application, Cryst. Growth Des. 9 (2009) 3532–3537.
[8] L. You, X. He, D. Wang, P. Sun, Y.F. Sun, X.S. Liang, Y. Du, G.Y. Lu, Ultrasensitive and low operating temperature NO_2 gas sensor using nanosheets assembled hierarchical WO_3 hollow microspheres, Sens. Actuators: B 173 (2012) 426–432.
[9] S.K. Lim, S.H. Hwang, D. Chang, S. Kim, Preparation of mesoporous In_2O_3 nanofibers by electrospinning and their application as a CO gas sensor, Sens. Actuators: B 149 (2010) 28–33.
[10] I.D. Kim, A. Rothschild, B.H. Lee, D.Y. Kim, S.M. Jo, H.L. Tuller, Ultrasensitive chemiresistors based on electrospun TiO_2 nanofibers, Nano Lett. 6 (2006) 2009–2013.
[11] D.P. Volanti, A.A. Felix, M.O. Orlandi, G. Whitfield, D.J. Yang, E. Longo, H.L. Tuller, J.A. Varela, The role of hierarchical morphologies in the superior gas sensing performance of CuO-based chemiresistors, Adv. Funct. Mater. 23 (2013) 1759–1766.
[12] Search on Web of Science® reveals over 1500 articles discussing SnO_2-based gas sensors.
[13] B. Wang, L.F. Zhu, Y.H. Yang, N.S. Xu, G.W. Yang, Fabrication of a SnO_2 nanowire gas sensor and sensor performance for hydrogen, J. Phys. Chem. C 112 (2008) 6643–6647.
[14] S.M. Sedghi, Y. Mortazavi, A. Khodadadi, Low temperature CO and CH_4 dual selective gas sensor using SnO_2 quantum dots prepared by sonochemical method, Sens. Actuators: B 145 (2010) 7–12.
[15] N.G. Cho, D.J. Yang, M.J. Jin, H.G. Kim, H.L. Tuller, I.D. Kim, Highly sensitive SnO_2 hollow nanofiber-based NO_2 gas sensors, Sens. Actuators: B 160 (2011) 1468–1472.
[16] Z.P. Li, Q.Q. Zhao, W.L. Fan, J.H. Zhan, Porous SnO_2 nanospheres as sensitive gas sensors for volatile organic compounds detection, Nanoscale 3 (2011) 1646–1652.
[17] P.H. Suman, A.A. Felix, H.L. Tuller, J.A. Varela, M.O. Orlandi, Giant chemoresistance of SnO disk-like structures, Sens. Actuators: B 186 (2013) 103–108.
[18] P.H. Suman, E. Longo, J.A. Varela, M.O. Orlandi, Controlled synthesis of layered Sn_3O_4 nanobelts by carbothermal reduction method and their gas sensor properties, J. Nanosci. Nanotechnol. 14 (2014) 6662–6668.
[19] V.X. Hien, J.-H. Lee, J.-J. Kin, Y.-W. Heo, Structure and NH_3 sensing properties of SnO thin film deposited by RF magnetron sputtering, Sens. Actuators: B 194 (2014) 134–141.
[20] Z.R. Dai, Z.W. Pan, Z.L. Wang, Growth and structure evolution of novel tin oxide diskettes, J. Am. Chem. Soc. 124 (2002) 8673–8680.
[21] M.O. Orlandi, A.J. Ramirez, E.R. Leite, E. Longo, Morphological evolution of tin oxide nanobelts after phase transition, Cryst. Growth Des. 8 (2008) 1067–1072.
[22] G.V. Samsonov, The Oxide Handbook, Plenum Press, New York, 1973.
[23] Y. Ogo, H. Hiramatsu, K. Nomura, H. Yanagi, T. Kamiya, M. Hirano, H. Hosono, p-channel thin-film transistor using p-type oxide semiconductor, SnO, Appl. Phys. Lett. 93 (2008) 032113.
[24] M.O. Orlandi, E.R. Leite, R. Aguiar, J. Bettini, E. Longo, Growth of SnO nanobelts and dendrites by a self-catalytic VLS process, J. Phys. Chem. B 110 (2006) 6621–6625.
[25] M. Batzill, U. Diebold, The surface and materials science of tin oxide, Prog. Surf. Sci. 79 (2005) 47–154.
[26] P.H. Suman, M.O. Orlandi, Influence of processing parameters on nanomaterials synthesis efficiency by a carbothermal reduction process, J. Nanopart. Res. 13 (2011) 2081–2088.
[27] S. Brunauer, P.H. Emmett, E. Teller, Adsorption of gases in multimolecular layers, J. Am. Chem. Soc. 60 (1938) 309–319.
[28] J.L.G. Fierro, Metal Oxides: Chemistry and Applications, CRC Press, Boca Raton, 2013.
[29] R. Waser, Nanoelectronics and Information Technology, Wiley-VCH, Weinheim, 2005.
[30] R.S. Wagner, W.C. Ellis, Vapor–liquid–solid mechanism of single crystal growth, Appl. Phys. Lett. 4 (1964) 89–90.
[31] Z.W. Pan, Z.R. Dai, Z.L. Wang, Nanobelts of semiconducting oxides, Science 291 (2001) 1947–1949.
[32] X. Wang, W. Liu, H. Yang, X. Li, N. Li, R. Shi, H. Zhao, J. Yu, Low-temperature vapor–solid growth and excellent field emission performance of highly oriented SnO_2 nanorod arrays, Acta Mater. 59 (2011) 1291–1299.
[33] L.Y. Liang, Z.M. Liu, H.T. Cao, Z. Yu, Y.Y. Shi, A.H. Chen, H.Z. Zhang, Y.Q. Fang, X.L. Sun, Phase and optical characterizations of annealed SnO thin films and their p-type TFT application, J. Electrochem. Soc. 157 (2010) H598–H602.
[34] U.S. Environmental Protection Agency: National Ambient Air Quality Standards (NAAQS), 2014, http://www.epa.gov/air/criteria.html
[35] N. Barsan, U. Weimar, Conduction model of metal oxide gas sensors, J. Electroceram. 7 (2001) 143–167.
[36] K. Sahner, H.L. Tuller, Novel deposition techniques for metal oxide: Prospects for gas sensing, J. Electroceram. 24 (2010) 177–199.
[37] G.J. Li, X.H. Zhang, S. Kawi, Relationships between sensitivity, catalytic activity, and surface areas of SnO_2 gas sensors, Sens. Actuators: B 60 (1999) 64–70.
[38] K.S.W. Sing, Reporting physisorption data for gas solid systems – with special reference to the determination of surface-area and porosity, Pure Appl. Chem. 54 (1982) 2201–2218.
[39] A. Walsh, G.W. Watson, Electronic structures of rocksalt, litharge, and herzenbergite SnO by density functional theory, Phys. Rev. B 70 (2004) 235114.

[40] A. Seko, A. Togo, F. Oba, I. Tanaka, Structure and stability of a homologous series of tin oxides, Phys. Rev. Lett. 100 (2008) 045702.

Biographies

Pedro H. Suman received his degree in Physics from São Paulo State University (2009) and his Master degree in Materials Science and Technology also from São Paulo State University (2012). He is currently a Ph.D. student at São Paulo State University under supervision of Prof. Marcelo O. Orlandi. His research interest is mainly about the synthesis of semiconductor nanostructured materials for gas sensor applications.

Anderson A. Felix received his physics undergraduate degree (2006) and master science degree in materials science (2009) from Faculty of Engineering at São Paulo State University (2009). He has been a Ph.D. Student in Chemistry Institute at São Paulo State University. At present he is working with Prof. Harry L. Tuller as a visiting student at the Department of Materials Science and Engineering at MIT. His research interests are centered mainly in the fields of novel nanomaterial architectures for application as chemical sensors.

Harry L. Tuller received his S.B. and S.M. degrees in electrical engineering and his EngScD in solid state science and engineering from Columbia University in New York. He is a member of the faculty of the Department of Materials Science and Engineering at MIT, where he serves as professor of ceramics and electronic materials and director of the Crystal Physics and Electroceramics Laboratory. Dr. Tuller's current research emphasizes the integration of sensor and actuator materials into microelectromechanical (MEMS) and microphotonic systems and the modeling, processing, characterization and optimization of solid state ionic devices (sensors, batteries, fuel cells). He has published over 425 articles, coedited 15 books and been awarded 29 patents. Dr. Tuller is editor-in-chief of the Journal of Electroceramics and series editor of Electronic Materials: Science and Technology, Springer Academic Publishers. He is a fellow of the American Ceramic Society and the Electrochemical Society, recipient of Fulbright and von Humboldt Awards and former holder of the Sumitomo Electric Industries Faculty Chair at MIT. Dr. Tuller was awarded Docteur Honoris Causa (2004), for life-long contributions to the field of electroceramics by the University of Provence, Marseilles, France and Docteur Honoris Causa (2009) from the University of Oulu, Finland. Dr. Tuller is co-founder of Boston MicroSystems Inc., a pioneer in the design and fabrication of harsh environment compatible micromachined Si and SiC-based sensor arrays.

José A. Varela is graduated in Physics from University of São Paulo (1968), and received his Master Degree in Physics from Technological Institute of Aeronautics (1975) both in Brazil. He received Ph.D. in Materials Science from University of Washington, Seattle, WA, USA in 1981. He has been Professor at University of São Paulo State – UNESP, Brazil since 1983. His main research interests are microwave assisted hydrothermal synthesis of inorganic materials as well as ceramic thin films chemical and physical deposition for applications including ferroelectrics, varistors, electro-optical and sensors.

Marcelo O. Orlandi is physicist with Ph.D. in Material Science and Engineering field by Federal University of São Carlos (2005). Currently he has been a professor at São Paulo State University. In the last few years the main focus of Dr. Orlandi research has been the controllable growth and modeling of nanomaterials and the sensor response of nanomaterials. Other areas of interest are transport in nanomaterials and electron microscopy.